

Oriented monazite inclusions in apatite porphyroblasts from the Hemlo gold deposit, Ontario, Canada

YUANMING PAN, MICHAEL E. FLEET AND NEIL D. MACRAE

Department of Geology University of Western Ontario London, Ontario N6A 5B7, Canada

Abstract

Oriented inclusions of monazite occur in the dark core of apatite porphyroblasts in a muscovite schist from the Archaean Hemlo gold deposit, Ontario, Canada. The monazite inclusions are elongated along the *b*-axis and parallel to the *c*-axis of the apatite host; the complete orientation relationship of the monazite/apatite intergrowth is *bMnz//cAp*, *cMnz//aAp*. From analysis by SIMS and EMP, the dark core of the apatite porphyroblasts is depleted in *LREE* ($La_N/Yb_N = 0.56$). The monazite inclusions are correspondingly enriched in *LREE*, but markedly depleted in *HREE*, compared with monazite grains in the rock matrix and cross-cutting veins. The monazite inclusions precipitated by oriented reaction through rock–fluid interactions during a late hydrothermal alteration. Their unusual *REE* composition is probably related to both a preferential leaching of *LREE* from the dark core and a selective transfer of *HREE* out of the apatite porphyroblasts.

KEYWORDS: apatite porphyroblasts, monazite, oriented intergrowth, rare earth elements.

Introduction

Oriented intergrowths of rare earth minerals are not uncommon (Mariano, 1989); the 'syntaxy' or 'polycrystals' of bastnäsite, parisite, röntgenite and synchisite are perhaps the best-known examples (Donnay and Donnay, 1953; Van Landuyt and Amelinckx, 1975). The structure of apatite-group minerals [$Ca_5(PO_4)_3(OH, F, Cl)$] accommodates a variable quantity of rare earth elements (*REE*) as isomorphous substitutions for Ca (Deer *et al.*, 1962; Fleischer and Altschuler, 1986; Roeder *et al.*, 1987; Ronsbo, 1989; Hughes *et al.*, 1991). Atomic substitution by *REE* is usually represented as either $Ca^{2+} + P^{5+} = REE^{3+} + Si^{4+}$ or $2Ca^{2+} = REE^{3+} + Na^+$ (Ronsbo, 1989). Additionally, apatite commonly contains inclusions of rare earth minerals (e.g. bastnäsite and monazite) and *REE*-bearing minerals (e.g. xenotime and zircon; cf. Deer *et al.*, 1962; Åmli, 1975; Boudreau and McCallum, 1990). In particular, Åmli (1975) reported that elongated prismatic grains of xenotime in apatite from the Gloserheia granite pegmatite from southern Norway are oriented with the *c*-axis parallel to the *c*-axis of the host. More generally, Åmli (op. cit.) also noted elongated

prismatic quartz and plagioclase inclusions parallel to the *c*-axis of apatite. Taborszky (1962) reported zircon, hornblende, and mica inclusions, mostly oriented parallel to the *c*-axis of apatite, in granitic to gabbroic rocks of the Odenwald province, Germany, and Pignorini and Veniale (1968) reported long prismatic inclusions of monazite, xenotime, plagioclase (?) and biotite oriented parallel to the *c*-axis of apatite in granitic to granodioritic rocks of the Val Sersera province, Italy.

The present paper reports on *REE*-bearing metamorphic apatite from the Hemlo gold deposit, Ontario, Canada, that occurs as porphyroblasts with oriented monazite inclusions in the ore zones, and with a dark pleochroic core in the hanging-wall. The orientation relationship of the monazite/apatite intergrowth is established from optical petrography and single-crystal X-ray precession study. In addition, textural evidence, available U/Pb geochronological data (Corfu and Muir, 1989), and *REE* compositions of monazite and apatite, determined by electron microprobe (EMP) analysis and secondary ion mass spectrometry (SIMS), respectively, are used to discuss possible mechanisms for the formation of monazite inclusions in apatite.

Occurrence and petrography

The monazite/apatite intergrowth was observed in a muscovite schist from the Highway zone of the Golden Sceptre Resources Limited property, which is part of the diffuse westward extension of the Hemlo gold deposit (Pan and Fleet, 1991a; 1992). The pleochroic apatite was observed in a staurolite-bearing metapelite from the hanging-wall of the Golden Giant mine at the Hemlo deposit (cf. Goad, 1987). The Hemlo gold deposit is located approximately 35 km east of Marathon, Ontario, Canada, contains approximately 80 Mt of ore with an average grade of 7.7 g/t Au (Harris, 1989), and hosts the three biggest gold mines currently in production in Canada, namely the Williams mine, the Golden Giant mine and the David Bell mine.

The Hemlo gold deposit is situated within the late Archaean Hemlo–Heron Bay greenstone belt which is comprised predominantly of a sequence of highly metamorphosed and deformed sedimentary and volcanic rocks. All supracrustal rocks of the Hemlo–Heron Bay greenstone belt have been subjected to a complex history of deposition, deformation, metamorphism, magmatism and hydrothermal alteration (Corfu and Muir, 1989; Pan and Fleet, 1991a; 1992 and references therein). The peak regional metamorphism at the Hemlo gold deposit reached middle amphibolite facies conditions (Pan and Fleet, 1991a). Hydrothermal alteration following the peak regional metamorphism at the Hemlo gold deposit included an intensive and extensive potassic event (Pan and Fleet, 1991a; 1992), dated by Masliwec *et al.* (1986) at 2671 ± 5 Ma, and a late calc-silicate alteration (Pan and Fleet, 1991a; 1992).

The muscovite schist exhibits a well-developed schistosity, defined by both a preferred orientation of micas and an alternation of micaceous and quartzofeldspathic layers, and is composed of muscovite, quartz, plagioclase, microcline, biotite, apatite, monazite, tourmaline, and pyrite. Similar to many other ore-bearing rock types of the Hemlo gold deposit (Pan and Fleet, 1991a), the muscovite schist contains large deformed quartz and partly altered oligoclase grains (commonly referred to as quartz and oligoclase 'eyes' by local geologists), which have been interpreted to be relict phenocrysts (Pan and Fleet, 1991a). Several cross-cutting veins (< 1 cm wide) of quartz, with accessory calcite, pyrite, apatite, and monazite, are also present in the muscovite schist.

The monazite/apatite intergrowths are generally restricted to a single quartz-rich layer about 0.5 cm wide and occur as porphyroblasts of various sizes (up to 1 mm in diameter) surrounded

by a fine-grained, foliated, micaceous groundmass (a typical 'augen' texture; Fig. 1a). The apatite porphyroblasts are commonly stubby {1010} prisms and are characterised by an obvious zonation with a dark inclusion-filled core and a narrow clear margin (Fig. 1a). Several apatite porphyroblasts also have late fractures filled in by clear apatite.

Acicular, oriented inclusions along the {1010} cleavage partings of the apatite porphyroblasts are unevenly distributed within the dark core and are readily observed by optical microscopy (Fig. 1b) and back-scattered electron imaging (Fig. 1c). These inclusions commonly represent no more than 1 modal % of the apatite porphyroblasts and are generally less than 1 μm in width but may exceed 100 μm in length. X-ray diffraction studies and EMP analysis established that they are monazite. Some EMP analyses are consistent with rhabdophane (see below), but this is not confirmed by X-ray diffraction. Grains of REE phosphate (believed to be either monazite or rhabdophane) are also present along fractures across the dark core (Fig. 1c). No rare earth mineral inclusions were observed in the clear areas (margin and fractures) of the apatite porphyroblasts. Other minerals, such as quartz and plagioclase, are present as inclusions in all parts of the apatite porphyroblasts but are apparently randomly distributed.

Apatite in the staurolite-bearing metapelite from the hanging-wall of the Golden Giant mine occurs in both the rock matrix (Fig. 1d) and as mineral inclusions within staurolite porphyroblasts and is also characterised by a dark (almost opaque) core and a clear rim (Fig. 1d). A few minute rod-like inclusions are present in the dark core but rare earth mineral inclusions have not been confirmed. The dark core of these apatite grains is pleochroic, and its boundary follows crystal growth outlines (Fig. 1d).

Monazite is also present as small isolated grains in the matrix and cross-cutting quartz veins of the muscovite schist, and has been found to be a common but minor phase in both the matrix and cross-cutting veins in other ore-bearing rock types of the Hemlo gold deposit. However, rhabdophane is absent in the matrix and cross-cutting veins of the muscovite schist.

Crystallographic orientation

Weak 120 reflections of monazite were evident in zero-level, *a*-axis precession films of apatite grains removed from polished thin-sections (Fig. 2). Monazite 200 reflections were also present, but partly obscured by a white radiation streak.

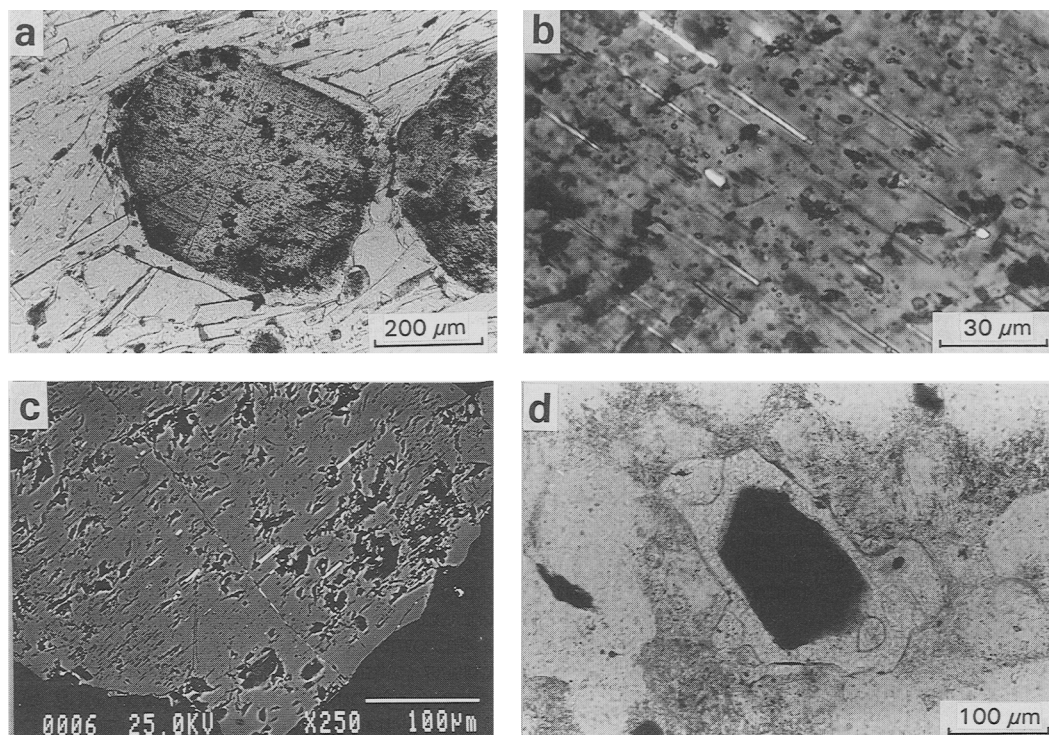


FIG. 1. Photomicrographs (*a*, *b*, *d*) and back-scattered electron image (*c*) showing apatite from the Hemlo gold deposit: (*a*) apatite porphyroblasts with a dark core and a narrow clear margin in muscovite schist from the ore zone; (*b*) acicular, oriented inclusions of monazite in the dark core of an apatite porphyroblast in muscovite schist; (*c*) monazite inclusions (white) in an apatite porphyroblast in muscovite schist; note monazite inclusions also occur along the fracture through the dark core; (*d*) apatite with a pleochroic dark core and a clear margin in the matrix of staurolite-bearing metapelite from the hanging-wall.

Thus, the orientation relationship of the composite diffraction pattern is $b^*Mnz//c^*Ap$, $a^*Mnz//a^*Ap$. This corresponds to $bMnz//cAp$, $cMnz//aAp$ for the monazite/apatite intergrowth.

Monazite 120 reflections were not equally intense for all equivalent orientations about the c^* -axis of apatite, suggesting that equivalent orientations of the intergrowth were not equally developed. Also, grains oriented by X-ray precision and then examined microscopically using a spindle stage revealed that the acicular monazite inclusions tend to be flattened normal to the $bMnz$, $cMnz$ plane. Thus, the monazite inclusions are elongated along the $bMnz$ -axis (parallel to the c -axis of the apatite host), and are marginally flattened in the (100) Mnz plane. Typical, isolated monazite crystals do tend to be flattened on (100), but are generally more elongated along the c -axis rather than the b -axis. However, the shape of the present acicular inclusions is not inconsistent with the cleavage and growth habits of monazite (cf. Deer *et al.*, 1962).

Chemical compositions

Major element compositions of apatite and monazite, including *REE* in the latter, were determined using a JEOL JXA-8600 Superprobe fitted with four automated wavelength-dispersive spectrometers, at the University of Western Ontario (UWO). Operating conditions included an accelerating voltage of 25 kV, a beam current of 20 nA, beam diameter of 2–5 μm , 20s counts, and minerals and synthetic glasses as standards (cf. Pan and Fleet, 1990; 1991b).

REE in apatite were analysed by secondary ion mass spectrometry (SIMS) using the CAMECA IMS 3f instrument at Surface Science Western, UWO. The same polished thin sections used for EMP analyses were used here, but coated with approximately 400Å of gold rather than carbon. For all analyses, the $^{16}\text{O}^-$ primary beam was mass filtered, accelerated by 12.5 kV and focused to produce (over the total run time per spot of 26.7 minutes) a sputter crater measuring approxima-

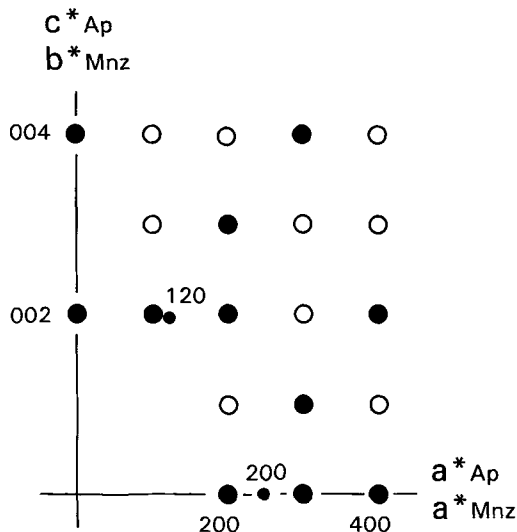


FIG. 2. Interpretation of part of a precession photograph of an apatite grain with monazite acicular inclusions from muscovite schist: Mo-K α ; $\mu = 20^\circ$; zero level; Ap, apatite; Mnz, monazite; precession axis is a^*Ap ; large circles are apatite reflections (solid, strong; open, others); small circles are monazite reflections, 200 of monazite is partly concealed by white radiation streak. Deduced orientation of monazite/apatite intergrowth is $bMnz//cAp$, $cMnz//aAp$.

tely 50 μm at the sample surface. Positive secondary ions were accelerated through a nominal 4.5 kV sample voltage, offset by -400 V . This extreme energy offset was chosen after noting evidence of molecular interferences [probably from F with light REE (*LREE*)] on the heavy REE (*HREE*) masses using the regular -100 V offset. Several analyses were then completed using the 'specimen isolation' (SI) technique, proven to eliminate molecular ions from non-conductive samples from spectra in the REE range (see MacRae, 1987; MacRae *et al.*, 1993). Because we required a primary beam size much less than that produced during SI analyses, we chose to retain the conventional analytical technique but increase the secondary ion offset voltage to a value where no evidence of interference was noted (i.e. values and trends comparable to those of SI analyses); this occurred at -400 V . Other instrumental parameters were identical to those documented in MacRae *et al.* (1993).

We counted for 20 seconds at each of the following masses: 42, 139, 140, 146, 149, 151, 153, 156, 158, 161, 162, 163, 167, 174, and 175. Backgrounds were checked at mass 174.5 and proved completely negligible, thus no back-

ground corrections were made. All intensities were corrected for isotopic abundances and normalised to Ca (analysed at mass 42) to correct for any instrumental variations. Because of the very large voltage offset, no molecular interference corrections were needed, and those very small interferences of Dy on Gd (at masses 156 and 158) were ignored. A similarly small overlap of Er on the Dy peak at 162 prompted us to average determinations from 161 and 163 for Dy and ignore 162.

Although intensities were measured for 5 cycles at each spot, data from only the last three were used in order to ensure steady state sputtering conditions. Precision for all intensity ratios was estimated to be better than 10%. REE/Ca values for the samples were standardised using the well-known apatite from Durango, Mexico, and the analyses recorded by Roelandts (1988) and Brunfelt and Roelandts (1974). The SIMS analytical craters were subsequently located by optical microscopy and back-scattered electron imaging in order to ensure that the analysed areas were indeed on the previously selected spots and remote from included phases.

Apatite. Representative combined EMP/SIMS compositions of apatite are given in Table 1. All apatites from the Hemlo gold deposit, including the zoned porphyroblasts of this study, are fluorapatite (Table 1; cf. Pan and Fleet, 1991a). The dark core of apatite porphyroblasts is apparently enriched in minor elements, such as Si, Mn, Fe, and Y, compared with the clear areas (margin and along fractures). However, minor amounts of Ba and Sr are present in both the dark core and the clear areas of the apatite porphyroblasts (Table 1). Apatite in the staurolite-bearing metapelite is also characterised by minor amounts of Ba and Sr (Table 1). These two elements are known to be anomalously concentrated in the Hemlo gold deposit (Harris, 1989) and its vicinity (Pan and Fleet, 1991c).

Fig. 3a shows that the dark core of the apatite porphyroblasts from the ore zone has a convex-upward chondrite-normalised REE pattern with a small positive Eu-anomaly [$\mathcal{L}n(Eu_N/Eu_N^*) = 0.23$, where $Eu_N^* = (Sm_N^*Gd_N^*)^{0.5}$]. A moderate depletion of *LREE* over *HREE* is indicated by $La_N/Yb_N = 0.56$. Unfortunately, an independent analysis for the small clear areas (margin and along fractures) of the apatite porphyroblasts was not possible due to the relatively large beam size of the present SIMS analysis. An overlapped SIMS spot with the dark core and clear margin at approximately 1:1 modal proportion yielded a similar convex-upward chondrite-normalised REE pattern but considerably lower absolute

Table 1. Compositions of apatite

Analysis	1	2	3	4
SiO ₂ (wt. %)	0.49	0.11	0.21	0.05
Al ₂ O ₃	0.21	0.02	0.12	0.00
FeO	0.12	0.02	0.22	0.00
MnO	0.06	0.00	0.44	0.10
CaO	54.17	54.13	55.09	55.01
BaO	0.35	0.32	0.21	0.11
SrO	0.41	0.35	0.53	0.13
Na ₂ O	0.15	0.11	0.00	0.00
P ₂ O ₅	40.83	40.76	40.67	40.99
Y ₂ O ₃	0.12	0.12	nd	nd
F	2.76	3.61	4.11	3.85
O=F	1.16	1.52	1.73	1.62
Total	98.74	99.03	99.87	98.62
formulae based on 12 oxygen atoms				
Si	0.040	0.009	0.017	0.004
Al	0.021	0.002	0.012	0.000
Fe	0.008	0.001	0.015	0.000
Mn	0.004	0.000	0.030	0.006
Ca	4.757	4.811	4.833	4.872
Ba	0.011	0.010	0.007	0.003
Sr	0.020	0.017	0.026	0.006
Na	0.023	0.018	0.000	0.000
P	2.828	2.857	2.814	2.864
Y	0.005	0.005	-----	-----
F	0.715	0.946	1.063	1.005
La (ppm) †	91	68 ^a	240	70 ^b
Ce	430	350	690	280
Nd	630	500	590	380
Sm	220	180	160	130
Eu	79	69	24	22
Gd	170	150	120	130
Dy	210	170	190	200
Er	94	73	85	92
Yb	110	76	90	76

- 1, dark core of apatite porphyroblast from ore zone;
 2, clear margin of apatite porphyroblast from ore zone;
 3, dark core of apatite in metapelite from hanging wall;
 4, clear margin of apatite in metapelite from hanging wall;
 wt. %, weight percent; nd, not determined;
 †, REEs by SIMS in parts per million (ppm);
^a, overlapped core-margin spot in apatite porphyroblast;
^b, overlapped core-margin spot in apatite in metapelite.

REE abundances, as compared to the dark core (Table 1; Fig. 3a). This may indicate that the clear areas of the apatite porphyroblasts have much lower REE concentrations than the dark core.

Fig. 3b shows that the pleochroic core of apatite grains in the staurolite-bearing metapelite has a slightly LREE-enriched ($La_N/Yb_N = 1.8$) pattern with a negative Eu-anomaly [$\mathcal{L}n(Eu_N/Eu_N^*) = -0.63$]. An analysis on an overlapped SIMS spot with the dark core and clear margin at approximately 3:1 modal proportion again yielded a much lower total REE content (mainly in LREE), resulting in a LREE-depleted pattern ($La_N/Yb_N = 0.62$) with a negative Eu-anomaly [$\mathcal{L}n(Eu_N/Eu_N^*) = -0.68$].

Monazite. Representative EMP analyses of

monazite are given in Table 2, and the REE compositions are reproduced in Fig. 4: analyses of monazite inclusions were obtained on grains 5–10 μ m wide. Isolated grains of monazite in the rock matrix and cross-cutting veins are identical in chemical composition, including REE, and are characterised by minor amounts of Y and Th (Table 2). However, monazite inclusions within the apatite porphyroblasts differ significantly from these isolated grains not only in minor elements, such as CaO, Y₂O₃ and ThO₂, but in REE composition as well. The former (inclusions) contain apparently higher CaO but lower Y₂O₃ and ThO₂ contents than the latter and are characterised by an unusual LREE-enrichment and a marked depletion in HREE (Fig. 4),

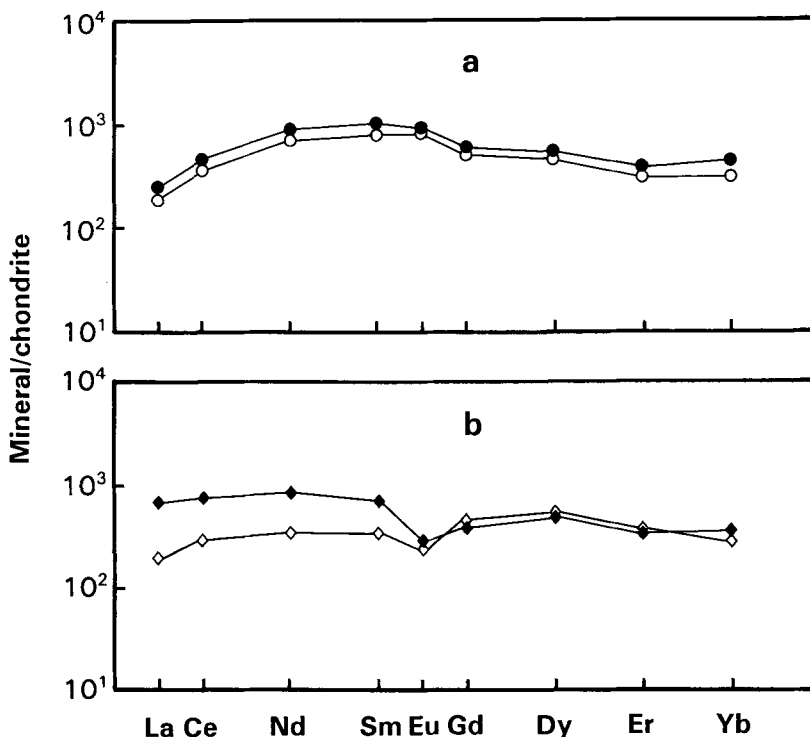


Fig. 3. Chondrite-normalised patterns showing rare-earth element compositions of: (a) apatite porphyroblasts in muscovite schist from the ore zone (solid circles, the dark inclusion-filled core; open circles, combined dark core-clear margin resulting from the overlapped SIMS spot; see text); (b) apatite in staurolite-bearing metapelite from the hanging-wall (solid diamonds, the dark pleochroic core; open diamonds, combined dark core-clear margin resulting from the overlapped SIMS spot; see text).

whereas the isolated grains of monazite in the matrix and cross-cutting veins are also *LREE*-enriched but are only moderately depleted in *HREE* (Fig. 4).

Several inclusions in the apatite porphyroblasts of the muscovite schist yielded EMP results with a monazite-type $\Sigma REE/P$ atomic proportion (i.e. 1:1) but much less than 100% in oxide totals (Table 2). These results are either related to analytical difficulties due to the extremely small grain size or represent a hydrous phase, possibly, rhabdophane ($REEPO_4 \cdot nH_2O$). However, as noted above, X-ray single-crystal precession and powder diffraction studies failed to detect rhabdophane or any other $REEPO_4 \cdot nH_2O$ mineral in the apatite porphyroblasts.

Discussion and conclusions

Monazite/apatite intergrowth. As discussed in Fleet (1982) and Fleet and Arima (1985), the dominant factors controlling the shape and orientation of crystalline precipitates and replacement

products in minerals is minimisation of interfacial energy. Thus, oriented inclusions tend to have either a topotactic relationship with the matrix phase or an orientation which minimises the dimensional misfit between the strain-free lattices at the phase boundary. The nomenclature of oriented intergrowths was reconsidered by Bernal and Mackay (1965). They suggested that the term 'topotaxy' should be restricted to an intergrowth of two or more phases with mutual, three-dimensional orientation, when it is suspected that dimensional and structural correspondences in the three axial directions also exist. Lattice coherence is not required. Unfortunately, there are numerous intergrowths involving precipitates and replacement products which have mutual, three-dimensional orientation but lack the requisite dimensional and structural correspondences in all three axial directions. Such intergrowths are commonly also referred to as 'topotactic' (e.g. Fleet and Arima, 1985; Shau *et al.*, 1991). In the absence of specific terminology, we will refer to these intergrowths as 'topotactic-like'.

Table 2. Compositions of monazite

Analysis	1	2	3
SiO ₂ (wt. %)	0.00	0.00	0.00
Al ₂ O ₃	0.00	0.00	0.00
FeO	0.00	0.00	0.00
MnO	0.00	0.00	0.00
CaO	1.52	0.39	0.83
Na ₂ O	0.00	0.00	0.00
P ₂ O ₅	29.79	29.13	28.18
La ₂ O ₃	13.29	15.18	13.01
Ce ₂ O ₃	36.29	30.86	35.72
Pr ₂ O ₃	3.99	3.52	3.35
Nd ₂ O ₃	14.12	13.47	12.30
Sm ₂ O ₃	0.80	2.44	0.69
Eu ₂ O ₃	0.00	0.31	0.00
Gd ₂ O ₃	0.21	1.51	0.10
Dy ₂ O ₃	0.10	0.64	0.05
Yb ₂ O ₃	0.00	0.00	0.00
Y ₂ O ₃	0.15	0.53	0.10
ThO ₂	0.07	1.13	0.06
Total	100.23	99.32	94.39
formulae based on 4 oxygen atoms			
Ca	0.064	0.017	0.037
P	0.985	0.986	0.992
ΣREE	0.983	0.998	0.982

1, monazite inclusion in apatite from ore zone;
 2, isolated monazite grain in the matrix;
 3, unidentified inclusion (rhabdophane ?);
 wt. %, weight percent.

As noted in Fleet and Arima (1985), topotaxy involves a shared structural element and therefore topotactic phase boundaries are usually rational planes. Their orientation is independent of the precise values of the strain-free lattice parameters. On the other hand, phase boundaries defined by minimisation of lattice misfit are, in general, irrational, and their orientation is sensitive to change in lattice parameters through change in temperature, pressure, composition, and so on. Dimensional (lattice) misfit boundaries may be either coincident or simply optimal, and have indices (hkL) common to both lattices (Fleet, 1982). They are more characteristically associated with a matrix phase of low symmetry (triclinic and monoclinic), whereas topotactic boundaries are associated with a matrix phase of higher symmetry. Thus, magnetite inclusions in augite were observed to have coincident phase boundaries (Fleet *et al.*, 1980) and to be completely analogous to the more familiar intergrowths of isomorphous monoclinic chain silicates (e.g. Robinson *et al.*, 1977). However, where the matrix phase is cubic, as in the recently reported chlorite/chromite intergrowth (Fleet *et al.*, 1993), previous experience suggests that the intergrowth orientation should be controlled by topotaxy.

This is readily demonstrated by the lack of close dimensional correspondence between equivalent lattices of the two phases and by the absence of lattice rotation.

Oriented intergrowths with a topotactic phase boundary frequently involve a shared structural element as an important feature in the interface structure. As in the chlorite/chromite and chlorite/olivine intergrowths (Fleet *et al.*, 1993), this is commonly a layer of closest-packed anions. However, in topotactic-like intergrowths the interface structure is not always readily apparent and, in cases where no structural similarity is evident, may not be extensively present; that is, the actual phase boundary may be more like a sub-grain or grain boundary. This may be illustrated by the recent study of oriented rutile and titanite inclusions in sagenitic biotite (Shau *et al.*, 1991). Rutile needles have a single preferred orientation related to the pseudohexagonal symmetry of the biotite host, and the two coexisting phases share nearly closest-packed anion layers and chains of edge-sharing octahedra. However, titanite inclusions exhibit several (non-equivalent) preferred orientations (one being dominant), and titanite does not have well-defined structural features in common with biotite.

Using unit-cell parameters for monazite and synthetic fluoroapatite from the JCPDS file, $bMnz = 6.97 \text{ \AA}$ and $cAp = 6.88 \text{ \AA}$, whereas $cMnz = 6.48 \text{ \AA}$ and $(2/3)aAp = 6.25 \text{ \AA}$. There is thus a poor correspondence between the lattices of monazite and apatite in the plane of the interface, particularly along $cMnz$, aAp . Additionally, there is no latticed rotation.

The only similarity in the crystal structures of monazite and apatite in the orientation of the intergrowth is in the layering of the phosphate groups normal to the b -axis of monazite and c -axis of apatite; there being two layers per structural repeat in each structure. The lack of equivalent structural features is perhaps not too surprising in view of the different stoichiometries of monazite and apatite, $Ce_3(PO_4)_3$ and $Ca_5(PO_4)_3(OH)$, respectively, and the absence of dominant closest-packed layers of anions in either structure.

Hence, the monazite inclusions appear to have been nucleated one-dimensionally from the favourable structural repeat along the c -axis of apatite. This would explain their pronounced b -axis elongation. We would not anticipate a well-developed interface structure in the interface plane (b , c of monazite), and it is probably no coincidence that the monazite inclusions are associated with a good $\{10\bar{1}0\}$ cleavage in the apatite host crystals. In summary, the monazite inclusions have precipitated by oriented reaction,

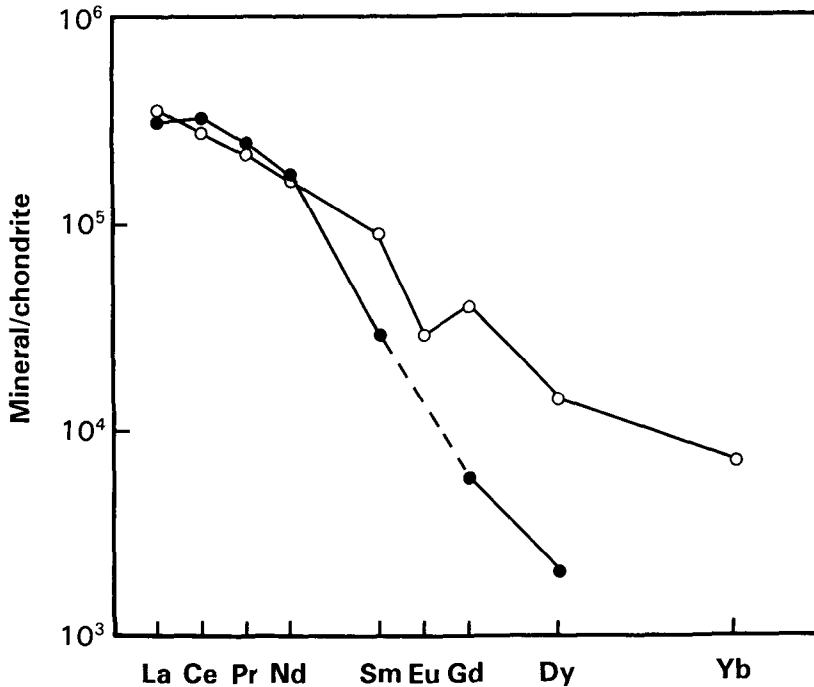


Fig. 4. Chondrite-normalised patterns illustrating rare-earth element compositions of monazite from the Hemlo gold deposit: solid circles represent monazite inclusions in apatite porphyroblasts from muscovite schist of the ore zone; open circles, isolated grains in the rock matrix.

but the monazite/apatite intergrowth is not rigorously topotactic.

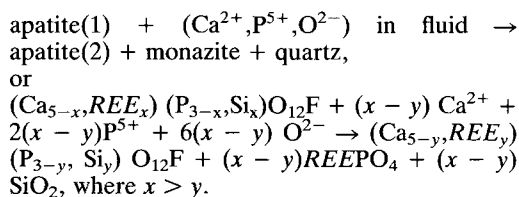
Origin of monazite inclusions. Åmli (1975) suggested that xenotime and monazite inclusions in apatite from the Gloserheia granite pegmatite, Norway formed by exsolution, possibly accompanied by metasomatism. He observed that xenotime inclusions in apatite differ in *REE* composition from other xenotimes and that the apatite close to xenotime inclusions is depleted in *REE*.

An igneous protolith is suggested for the muscovite schist of the ore zone at the Hemlo gold deposit, based on the well-preserved quartz and oligoclase phenocrysts and trace-element geochemistry (cf. Pan and Fleet, 1991a). However, the apatite porphyroblasts in the muscovite schist appear to have crystallised during the peak metamorphism of the region, because of their restricted occurrence within a quartz-rich band, the typical 'augen' texture, and the occurrence of similar zoned grains in close association with staurolite porphyroblasts in metapelite of the hanging-wall. Corfu and Muir (1989) obtained a ²⁰⁷Pb/²⁰⁶Pb age of 2670 Ma for apatite in an altered diorite dyke from the Hemlo gold deposit. The clear areas (margin and fracture filling) of the apatite porphyroblasts of this study are almost

certainly overgrowths formed late in the paragenetic sequence, and possibly during the late calc-silicate alteration associated with the gold mineralization, as clear apatite is a common minor phase in cross-cutting veins (Pan and Fleet, 1991a; 1992).

The formation of rare earth minerals, such as allanite, monazite, and synchiste, in the matrix and cross-cutting veins of the Hemlo gold deposit has been previously suggested to represent a local remobilisation and concentration of *REE* during the late calc-silicate alteration event (Pan and Fleet, 1991a; 1991b; 1992). The oriented inclusions of monazite in apatite porphyroblasts may also have crystallised during this late hydrothermal event. The low U and Th contents of all monazites of this study (Table 1) are indeed consistent with a hydrothermal origin (cf. Burnotte *et al.*, 1989). Additionally, the absence of rare earth mineral inclusions in apatite from the hanging-wall of the Golden Giant mine indicates the importance of hydrothermal fluid in the formation of monazite inclusions in apatite porphyroblasts within the ore zone. Corfu and Muir (1989) obtained relatively young U/Pb ages of 2637–2644 Ma for monazite from the Hemlo gold deposit.

The formation of monazite inclusions, (together with quartz inclusions) within the apatite porphyroblasts, may be represented by the following reaction:



This reaction emphasises communication with the hydrothermal fluid and includes stoichiometric apatites. The exsolution-only reactions of Åmli (1975) must invoke non-stoichiometric apatites. The common occurrence of apatite in cross-cutting veins and as a clear margin to apatite porphyroblasts indicates that Ca^{2+} and P^{5+} were readily available in the hydrothermal fluid, and a partial dissolution of the apatite porphyroblasts (cf. Pan *et al.*, 1993) would contribute P^{5+} (and Ca^{2+}) directly to the fluid for the formation of monazite inclusions. Other mineral inclusions, such as plagioclase, can also be included in the present reaction if additional constituents (e.g. Al) in apatite are taken into account.

It has long been known that secondary monazite forms during weathering from the release of *REE* from apatite and other minerals (Lottermoser, 1988; Mariano, 1989). The latter suggested that this involved an early stage of crystallisation of a hexagonal phase $\text{REEPO}_4 \cdot n\text{H}_2\text{O}$ (rhabdophane ?) followed by a late dehydration causing a conversion to anhydrous monoclinic monazite. The possible presence of a $\text{REEPO}_4 \cdot n\text{H}_2\text{O}$ phase in the apatite porphyroblasts of this study indicates similar processes may have been operative for the formation of acicular inclusions of monazite.

REE distribution. Published *REE* analyses (Fleischer and Altschular, 1986) indicate that apatite does not have a strong selectivity between *LREE* and *HREE*, although somewhat higher partition coefficients of *LREE* (particularly Nd) compared to *HREE* have been suggested by Hughes *et al.* (1991) based on a bond valence analysis. Instead, Fleischer and Altschular recognised that apatites in igneous rocks reflect their provenance in *REE* compositions. Available whole-rock *REE* data indicate that most ore-bearing rock types (including other muscovite schist samples), metasedimentary rocks and some intrusive rocks of the Hemlo gold deposit are characterised by marked *LREE*-enrichment (Pan and Fleet, 1991a). As noted above, the pleochroic apatite in staurolite-bearing metapelite is charac-

terised by a slight *LREE*-enrichment. The *LREE*-depleted patterns of the dark core of apatite porphyroblasts in the muscovite schist from the ore zone (Fig. 3a) cannot be directly attributed to their host-rock *REE* composition, but may be explained by a preferential leaching of *LREE* to form the *LREE*-enriched inclusions of monazite (below).

Monazite, on the other hand, is well-known for its preference for *LREE* (Murata *et al.*, 1953; Semenov, 1958; Felsche, 1976). The *REE* compositions of monazite in the matrix and cross-cutting veins of various rock types of the Hemlo gold deposit do indeed reflect their respective host-rock *REE* compositions (Pan and Fleet, 1990; 1991a). The distinct *REE* compositions of the monazite inclusions must then arise from their relationships with the host apatite porphyroblasts. In a separate study on the formation of rare earth minerals from titanite during late hydrothermal activity, Pan *et al.* (1993) observed that the titanite hosts are characterised by a prominent *LREE* depletion, whereas the rare earth minerals, including allanite, bastnäsite and monazite, in the alteration assemblages, are unusually enriched in *LREE* (and depleted in *HREE*). Mass-balance calculations indicated that a preferential leaching of *LREE* from the titanite hosts and a selective transfer of *HREE* out of the alteration assemblages both contributed to the *REE* compositions of the rare earth minerals (Pan *et al.*, 1993). Analogous processes probably contributed to the *REE* compositions of the monazite inclusions in the apatite porphyroblasts of this study. However, a direct evaluation of these two mechanisms (leaching and transfer) cannot be made in the present case because the original *REE* composition of the apatite host is unknown. The *REE* composition of the pleochroic core of the apatite from the hanging-wall (Table 1; Fig. 3b) is presumably pristine, but there is no basis for assuming that this is representative of the apatite porphyroblasts prior to their alteration.

A preferential leaching of *LREE* relative to *HREE* from the lattice of the apatite porphyroblasts from the ore zone is inferred from the marked *LREE* depletion of the dark core (Fig. 3a) and the formation of the unusually *LREE*-enriched monazite inclusions (Fig. 4). However, Watson *et al.* (1985) demonstrated experimentally that all *REE* have a similar diffusion rate in the apatite lattice at high-temperature but did caution any extrapolation to low-temperature. It is possible also that there was a selective transfer of *HREE* out of the apatite porphyroblasts, because of the increased stability of *REE* com-

plexes (fluorides, carbonates, etc.) with increasing atomic number (Wood, 1990; Pan *et al.*, 1993 and references therein) under hydrothermal conditions. It is noteworthy that HREE have almost certainly been leached from apatite in the Gloserheia granite pegmatite (Åmli, 1975) but were mainly fixed in xenotime inclusions within the apatite hosts. The absence of xenotime inclusions in the apatite porphyroblasts from the ore zone of the Hemlo gold deposit is probably attributable to the low Y-content of the host crystals (Table 1).

Acknowledgements

We thank D. M. Kingston and R. L. Barnett for assistance with electron microprobe analysis and Surface Science Western for the use of the CAMECA secondary ion mass spectrometer. The staurolite-bearing metapelite from the hanging wall of the Golden Giant mine was collected by R. E. Goad. Financial support for this research was provided by a Natural Sciences and Engineering Research Council (NSERC) of Canada research grant to MEF.

References

- Åmli, R. (1975) Mineralogy and rare earth geochemistry of apatite and xenotime from the Gloserheia granite pegmatite, Froland, southern Norway. *Am. Mineral.*, **60**, 607–20.
- Bernal, J. D. and Mackay, A. L. (1965) Topotaxy. *Tschermaks Min. Petr. Mitt.*, **10**, 331–40.
- Boudreau, A. E. and McCallum, I. S. (1990) Low-temperature alteration of REE-rich chlorapatite from the Stillwater Complex, Montana. *Am. Mineral.*, **75**, 687–93.
- Brunfelt, A. O. and Roelandts, I. (1974) Determination of rare earths and thorium in apatites by thermal and epithermal neutron-activation analysis. *Talanta*, **21**, 513–21.
- Burnotte, E., Picard, E., and Michel, G. (1989) Genesis of gray monazites: evidence from the Palaeozoic of Belgium. *Econ. Geol.*, **84**, 1417–29.
- Corfu, F. and Muir, T. L. (1989) The Hemlo–Heron Bay greenstone belt and the Hemlo Au–Mo deposit, Superior Province, Ontario, Canada. 2. Timing of metamorphism, alteration and Au mineralization from titanite, rutile, and monazite U–Pb geochronology. *Chem. Geol.*, **79**, 201–23.
- Deer, W. A., Howie, R. A., and Zussman, J. (1962) Non-silicates, Rock forming minerals, **5**, Non-silicates. Longman, London.
- Donnay, G. and Donnay, J. D. H. (1953) The crystallography of bastnaesite, parisite, roentgenite and synchisite. *Am. Mineral.*, **38**, 932–63.
- Felsche, J. (1976) Yttrium and lanthanides. In *Handbook of geochemistry* (Wedepohl, K. H. ed.), **II**, section 39, A1–42.
- Fleet, M. E. (1982) Orientation of phase and domain boundaries in crystalline solids. *Am. Mineral.*, **67**, 926–36.
- and Arima, M. (1985) Oriented hematite inclusions in sillimanite. *Ibid.*, **70**, 1232–7.
- Bilcox, G. A., and Barnett, R. L. (1980) Oriented magnetite inclusions in pyroxenes from the Grenville province. *Can. Mineral.*, **18**, 89–99.
- Angeli, N., and Pan, Y. (1993) Oriented chlorite lamellae in chromite from the Pedra Branca mafic-ultramafic complex, Ceará, Brazil. *Am. Mineral.*, **78**, 68–74.
- Fleischer, M. and Altschuler, Z. S. (1986) The lanthanides and yttrium in minerals of the apatite group—An analysis of the available data. *Neues Jahrb. Mineral., Mh.*, 467–80.
- Goad, R. E. (1987) *The geology, primary and secondary chemical dispersion of the Hemlo Au district metal occurrences, northwestern Ontario*. Unpubl. M.Sc. thesis, University of Western Ontario.
- Harris, D. C. (1989) The mineralogy and geochemistry of the Hemlo gold deposit. *Geol. Surv. Can., Econ. Geol. Rep.*, **38**, 88pp.
- Hughes, J. M., Cameron, M. and Mariano, A. N. (1991) Rare-earth-element ordering and structural variations in natural rare-earth-element-bearing apatites. *Am. Mineral.*, **76**, 1165–73.
- Lottermoser, B. G. (1988) Supergene, secondary monazite from the Mt. Weld carbonatite laterite, Western Australia. *Neues Jahrb. Mineral., Mh.*, 67–70.
- MacRae, N. D. (1987) Quantitative analysis of REEs by SIMS. *Am. Mineral.*, **72**, 1263–8.
- Bottazzi, P., Ottolini, L., and Vannucci, R. (1993) Quantitative REE analysis of silicates by SIMS: conventional energy filtering vs specimen isolation mode. *Chem. Geol.*, **103**, 45–54.
- Mariano, A. N. (1989) Economic geology of rare earth minerals. In *Geochemistry and mineralogy of rare earth elements* (B. R. Lipin and G. A. McKay, eds.), *Rev. Mineral.*, **21**, 308–37.
- Masliwec, A., McMaster, D. and York, D. (1986) The dating of Ontario's gold deposits. *Ontario Geol. Surv., Misc. Pap.*, **130**, 107–14.
- Murata, K. J., Rose, H. J. Jr., Carron, M. K., and Glass, J. J. (1957) Systematic variation of rare earth elements in cerium–earth minerals. *Geochim. Cosmochim. Acta*, **11**, 141–61.
- Pan, Y. and Fleet, M. E. (1990) Halogen-bearing allanite from the White River gold occurrence, Hemlo area, Ontario. *Can. Mineral.*, **28**, 67–75.
- (1991a) Metamorphic petrology and alteration assemblages of the Hemlo gold district. *Ontario Geol. Surv., Misc. Pap.*, **156**, 176–98.
- (1991b) Vanadian allanite-(La) and vanadian allanite-(Ce) from the Hemlo gold deposit, Ontario, Canada. *Mineral. Mag.*, **55**, 497–507.
- (1991c) Barian feldspar and barian-chromian muscovite from the Hemlo area, Ontario. *Can. Mineral.*, **29**, 481–96.
- (1992) Calc-silicate alteration in the Hemlo gold deposit, Ontario: mineral assemblages, P–T–X constraints and significance. *Econ. Geol.*, **87**, 1104–21.
- and MacRae, N. D. (1993) Late alteration in

- titanite (CaTiSiO_5): redistribution and remobilization of rare earth elements and implications for U/Pb and Th/Pb geochronology and nuclear waste disposal. *Geochim. Cosmochim. Acta*, **57**, 355–67.
- Pigorini, B. and Veniale, F. (1968) L'apatite accessoria nella diverse facies litologiche delle formazioni granitoidi della Val Sersera (Vercelli). *Rendiconti Soc. Ital. Mineral. Petro.*, **24**, 32pp.
- Robinson, P., Ros, M., Nord, G. C. Jr., Smyth, J. R. and Jaffe, H. W. (1977) Exsolution lamellae in augite and pigeonite: fossil indicators of lattice parameters at high-temperature and pressure. *Am. Mineral.*, **62**, 857–73.
- Roeder, P. L., MacArthur, D., Ma, X.-P., Palmer, G. R., and Mariano, A. N. (1987) Cathodoluminescence and microprobe study of rare-earth elements in apatite. *Ibid.*, **72**, 801–11.
- Roelandts, I. (1988) Comparison of inductively coupled plasma and neutron activation analysis for precise and accurate determination of nine rare-earth elements in geological materials. *Chem. Geol.*, **67**, 171–80.
- Ronsbo, J. G. (1989) Coupled substitutions involving REEs and Na and Si in apatites in alkaline rocks from the Ilimaussaq intrusion, South Greenland, and the petrological implications. *Am. Mineral.*, **74**, 896–901.
- Semenov, E. I. (1958) Relationship between composition of rare earths and structure of minerals. *Geochimiya*, **5**, 574–86.
- Shau, Y.-H., Yang, H.-Y. and Peacor, D. R. (1991) On oriented titanite and rutile inclusions in sagenitic biotite. *Am. Mineral.*, **76**, 1205–17.
- Taborszky, F. K. (1962) Geochimie des apatits in Tiefengesteinen am Beispiel des Odenwaldes. *Beitr. Mineral. Petrogr.*, **8**, 354–92.
- Van Landuyt, J. and Amelinckx, S. (1975) Multiple beam direct lattice imaging of new mixed-layer compounds of the bastnäsité-synchisite series. *Am. Mineral.*, **60**, 351–8.
- Watson, E. B., Harrison, T. M., and Ryerson, E. J. (1985) Diffusion of Sm, Sr, and Pb in fluorapatite. *Geochim. Cosmochim. Acta*, **49**, 1813–23.
- Wood, S. A. (1990) The aqueous geochemistry of the rare earth elements and yttrium. Part 2. Theoretical predictions of speciation in hydrothermal solutions to 350 °C at saturation water vapour pressure. *Chem. Geol.*, **88**, 99–125.

[Manuscript received 3 November 1992:
revised 4 March 1993]